Automatic Patient-Specific Microwave Ablation Planning Accelerated by a Physics-Guided Deep Learning Model

Seonaeng Cho[1], Minjee Seo[1], Minju Seol[1], Juil Park[2], Joon Ho Kwon[2], and Kyungho Yoon[1,3⋆]

[1] School of Mathematics and Computing (Computational Science and Engineering), Yonsei University, Seoul, Republic of Korea
yoonkh@yonsei.ac.kr
[2] College of Medicine, Department of Radiology, Yonsei University, Seoul, Republic of Korea
[3] Innovative & Intelligent Computational Science Institute (IN2CSI), Seoul, Republic of Korea

Abstract. Microwave ablation (MWA) is a promising minimally invasive treatment for liver tumors, but its therapeutic outcome strongly depends on patient-specific planning of antenna insertion trajectory, power, and treatment duration. Accurate numerical simulation can provide physically reliable ablation predictions; however, its high computational cost limits its use in optimization-based planning, where repeated forward evaluations are required. To address this issue, we propose a digital twin-based automatic planning framework that combines a neural ablation prediction model with a genetic algorithm. The model was trained on multiphysics simulation data generated from patient-specific tumor and vessel structures, antenna configurations, and treatment conditions, and was used as a fast forward model during planning. The prediction model achieved a Dice score of 95.1%, enabling accurate deep learning-based optimization. In 13 unseen planning cases, the proposed method improved ablation efficiency by 54.3% and shortened the antenna insertion trajectory length by 3.3% compared with clinician-defined planning, while maintaining broadly comparable target coverage and organ-damage levels. Most generated plans were also judged clinically applicable by MWA specialists. Furthermore, the framework enabled approximately 420-fold faster planning than numerical-simulation-based planning, demonstrating its potential as a fast digital twin for quantitative and personalized MWA treatment planning. The code is available at: https://github.com/SeonAengCho/MWA-Planning.git

Keywords: Microwave ablation · Treatment planning · Physics-Guided Deep Learning.

⋆ Corresponding author

1 Introduction

Microwave ablation (MWA) is a minimally invasive thermal therapy in which an antenna is inserted into the body to deliver microwave energy and induce thermal necrosis of tumor tissue [22]. Compared with surgical resection, which may be limited by general anesthesia, bleeding risk, and prolonged recovery, MWA can be performed through a percutaneous or small-incision approach [25, 9, 15]. Owing to these advantages, MWA has been increasingly adopted for the treatment of solid tumors, including liver tumors.

The therapeutic outcome of MWA, however, strongly depends on preoperative planning. Insufficient ablation may leave residual tumor tissue and increase the risk of local recurrence, whereas excessive ablation may damage surrounding normal tissues or critical organs [23, 12]. Therefore, preprocedural planning is essential to determine the antenna insertion position and trajectory, applied power, and treatment duration while accounting for the location, size, and shape of the tumor as well as nearby vessels and organs [13, 26].

In current clinical practice, MWA planning is often performed based on two-dimensional ultrasound or computed tomography (CT) images. Such image-guided planning makes it difficult to fully understand the three-dimensional spatial relationship between the tumor and surrounding anatomical structures, as well as the true tumor volume and morphology [1, 14]. In addition, treatment parameters are frequently selected based on manufacturer-provided protocol tables or empirical rules. These approaches do not sufficiently account for patient-specific tumor geometry, vascular structures, or heat-sink effects [5]. As a result, treatment planning remains highly operator-dependent and may not provide a systematic strategy for individualized therapy.

To overcome these limitations, patient-specific three-dimensional numerical simulations have been investigated to predict treatment outcomes [19, 6, 10], enabling simulation-based treatment planning [7, 17]. However, MWA simulation is a computationally expensive multiphysics problem that involves electromagnetic analysis, bioheat transfer, and thermal damage estimation. This computational burden becomes particularly problematic in optimization-based planning, where forward simulations must be repeatedly evaluated for various treatment parameters.

Recently, studies have sought to reduce this computational burden by training neural networks to approximate complex numerical simulation processes, thereby enabling faster inference [20]. In thermal therapy, Convolutional neural network (CNN)- or Transformer-based image models have been used to predict temperature distributions and ablation zones [21, 4], and neural operators have also been used to account for heat-sink effects [16]. In MWA, recent studies have explored the prediction of ablation zones from CT images and treatment conditions [11].

In this study, we propose a digital twin-based automatic MWA planning framework that combines a neural ablation prediction model with a genetic algorithm (GA). Ablation regions were generated using numerical multiphysics simulations based on patient-specific tumor and vessel structures, antenna configuration, power, and treatment duration. These data were used to train an affine transformation-based multimodal neural network, which was then used as a fast forward model within the optimization loop. The genetic algorithm searched for treatment plans on the patient-specific 3D body twin while considering feasible antenna trajectories, organ avoidance, normal tissue preservation, target coverage, and safety margin coverage. Through this framework, we propose a digital twin-based automatic MWA planning method with three main contributions: 1) personalized planning that reflects patient-specific tumor, vessel, and major anatomical structures, 2) reduced computational cost via neural network-based forward prediction, and 3) clinical applicability validated through quantitative comparison with clinician-defined planning and assessment by MWA specialists.

2 Method

2.1 Simulation-based Training Data Generation

Data acquisition We used the HepaticVessel dataset from the Medical Segmentation Decathlon [2], which provides abdominal CT images with liver tumor and intrahepatic vessel labels. A total of 60 patient CT datasets were used to train and test the neural ablation prediction model. These tumors exhibited substantial variability in size and morphology. Tumor volumes ranged from 353 to 11,540 mm^3, with a mean of $4,836.1 \pm 3,082.8$ mm^3. The sphericity ranged from 0.683 to 0.875, and the major-to-minor axis ratio ranged from 1.125 to 3.335. Tumor and vessel masks were separated, resampled to 1-mm isotropic spacing, and cropped into 81^3 volumes centered on each tumor centroid. For each tumor, 500 input conditions were randomly generated, including a six-dimensional antenna position and direction vector (x, y, z, dx, dy, dz) and a two-dimensional treatment vector consisting of power and duration. The antenna position was sampled within the tumor, while power and duration were sampled from 45–100 W and 60–300 s, respectively.

Numerical simulation Numerical simulations were performed for 30,000 generated input conditions to obtain the ablation regions. The simulation consisted of three multiphysics steps [3, 8]: electromagnetic field calculation using the Helmholtz equation, tissue temperature estimation using the Pennes bioheat equation, and cellular necrosis estimation using the Arrhenius model. The Helmholtz equation was solved using the finite element method (FEM), whereas the Pennes bioheat equation was solved using the finite difference method (FDM). The vessel region was maintained at 37°C, with a convection boundary condition applied at the vessel–tissue interface. Finally, the Arrhenius damage integral was accumulated over time, and voxels with a final value greater than 1 were defined as the necrotic region.

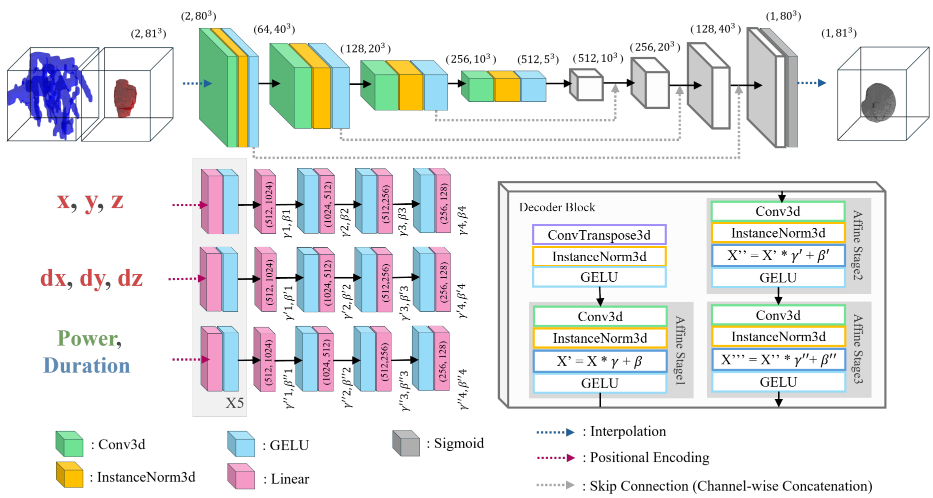

Fig. 1. Architecture of the neural ablation prediction model. Patient-specific tumor and vessel masks are encoded using a CNN encoder, while antenna configuration and treatment parameters are embedded to generate affine modulation parameters for decoder-stage feature conditioning.

2.2 Neural Ablation Prediction Model

The network architecture shown in Fig. 1 was designed to approximate the numerical simulation process described above. Accordingly, the model uses the same inputs and output as the numerical simulation and predicts the final ablation region from patient-specific tumor and vessel structures and treatment conditions.

The tumor-vessel volume was processed by a CNN-based encoder. The encoder repeatedly applies 3D CNN layers, instance normalization, and GELU activation to extract high-dimensional features while reducing the spatial resolution. The antenna position, antenna direction, power, and treatment duration were separately passed through positional encoding and linear layers to generate the affine parameters required at each decoder stage, namely the scale parameter γ and shift parameter β.

The extracted features and affine parameters were jointly used in the decoder blocks, allowing the feature maps to be modulated according to the treatment conditions. Each decoder block consists of one upsampling operation and three affine stages. In each affine stage, after a CNN layer, feature modulation was performed by applying γ and β to the feature map X as $X' = X \cdot \gamma + \beta$ [18]. The spatial resolution was progressively restored through four decoder blocks, and encoder features were combined with decoder features through skip connections using channel-wise concatenation.

Finally, the output was passed through a sigmoid function to obtain a probability map, which was thresholded at 0.5 to predict the final ablation region.

2.3 GA-based Treatment Planning

3D Body Twin Construction We performed GA-based planning to search for patient-specific MWA treatment parameters using the predicted ablation outcome. To account for anatomical constraints along the antenna insertion trajectory, a patient-specific 3D body twin was constructed from the original CT images. The rib region (HU $\geq$ 200) and body region (HU ≥ -500) were segmented in 3D Slicer, while major anatomical structures, including the aorta, veins, portal vein, colon, liver, pancreas, and stomach, were segmented using TotalSegmentator [24]. All segments were resampled to 1-mm voxel spacing and integrated into a single label map to construct the 3D body twin.

GA-based Optimization Method Before optimization, a 5 mm safety margin was added to the target tumor to generate the optimization target mask. The fitness function minimized by the GA was defined as Eq. 1. The objective function was designed such that the predicted ablation region maximally included the optimization target mask, and Eq. 2 represents the fraction of the target mask that was not ablated. The fraction of the ablated region corresponding to normal tissue, the vertical deflection angle defined as the angle from the horizontal plane, and the antenna insertion trajectory length through the body were treated as soft constraints. Each term was normalized between 0 and 1 and added to the GA fitness function as a weighted penalty term. In contrast, tumor coverage and collision between the antenna insertion trajectory and organs-at-risk were treated as hard constraints that must be satisfied, as defined in Eq. 4.

$$F(\mathbf{u}) = Obj(\mathbf{u}) + 0.3P_N(\mathbf{u}) + 0.3P_\theta(\mathbf{u}) + 0.3P_L(\mathbf{u}) \tag{1}$$

$$Obj(\mathbf{u}) = 1 - \frac{\sum_i M_i \hat{A}_i(\mathbf{u})}{\sum_i M_i + \epsilon} \tag{2}$$

$$P_N(\mathbf{u}) = \frac{\sum_i N_i \hat{A}_i(\mathbf{u})}{\sum_i \hat{A}_i(\mathbf{u}) + \epsilon} \tag{3}$$

$$\frac{\sum_i \hat{A}_i(\mathbf{u}) T_i}{\sum_i T_i} = 1, \qquad \sum_i R_i(\mathbf{u}) O_i = 0. \tag{4}$$

In Eqs. 1–4, $\hat{A}_i(\mathbf{u})$ denotes the thresholded binary ablation mask at voxel i for the optimization variable $\mathbf{u}$, obtained by applying a threshold of 0.5 to the model output. M_i and T_i denote the safety-margin-included target mask and the original tumor mask, respectively. N_i denotes the normal tissue mask, defined as the entire domain excluding the target mask, and $P_N(\mathbf{u})$ penalizes the fraction of the predicted ablation region corresponding to normal tissue. $P_\theta(\mathbf{u})$ and $P_L(\mathbf{u})$ denote the normalized penalties for the vertical deflection angle and antenna insertion trajectory length, respectively. The three penalty terms were empirically assigned equal weights of 0.3, allowing them to guide the optimization without overriding the primary objective or imposing additional preference among the auxiliary criteria.

In the hard constraints, complete tumor coverage was enforced by setting the tumor coverage ratio to 1. O_i denotes the organs-at-risk mask excluding the liver, and $R_i(\mathbf{u})$ denotes the antenna insertion trajectory mask.

The optimization variables $\mathbf{u}$ included the antenna position, insertion direction, applied power, and treatment duration. During optimization, the patient-specific tumor and vessel masks were fixed, while $\mathbf{u}$ was updated using the neural ablation prediction model trained in Section 2.2. The GA was run with a population size of 40 for 60 generations, using elitism for the best 4 candidates, tournament selection with a size of 3, blend crossover, and Gaussian mutation with a mutation rate of 0.25 and a mutation scale of 0.1.

3 Results

3.1 Ablation Zone Prediction Performance

The 60 patient CT datasets used for neural ablation prediction model training and evaluation were divided into training, validation, and test sets with 36, 12, and 12 datasets, respectively. To reduce bias in the data distribution, the datasets were sorted based on tumor size and the number of vessel voxels in the vessel mask, and then evenly distributed across the three sets. The validation set was used for early stopping with a patience of 5 to prevent overfitting during training. Ablation zone prediction performance was evaluated using 1,000 cases randomly sampled from the test set. The model achieved a Dice score of 95.06% and an IoU of 90.78%, showing high agreement between the predicted ablation zones and the numerical simulation results.

3.2 Planning Results

Evaluation Metrics Planning performance was evaluated using four quantitative metrics: ablation efficiency (AE), complete coverage (CP), organ damage rate (OD), and insertion path length (IPL). AE measured the proportion of the target mask within the simulated ablation region, while CP measured the coverage of the margin-included target mask by the ablation region. OD represented the proportion of the ablated region overlapping with organs-at-risk, and IPL was defined as the length of the antenna insertion trajectory inside the body mask. Higher AE and CP indicate better target ablation, whereas lower OD and IPL indicate safer and less invasive planning.

Quantitative Planning Performance For planning performance evaluation, 13 patients with liver tumors who were not used for training the prediction model were selected. The selected patients had a maximum tumor diameter of 40 mm or less, with a mean diameter of 21.8 mm (range: 7–36 mm). As a baseline, a clinician specializing in liver tumor MWA procedures was asked to perform conventional clinical planning based on CT images. The same neural ablation prediction model was then applied to the clinician-defined planning conditions to derive the predicted ablation outcomes.

Table 1 presents a quantitative comparison of the proposed and clinician-defined planning methods. The mean AE was higher for the proposed planning method than for clinician-defined planning (0.764 vs. 0.495), indicating that the ablation region was more efficiently concentrated within the target mask. The proposed planning method showed a slightly higher mean CP than clinician-defined planning (0.956 vs. 0.944), indicating that both methods achieved strong target coverage. The mean OD was low for both the proposed planning method and clinician-defined planning (0.014 vs. 0.011), indicating minimal damage to surrounding critical organs. In addition, the mean IPL was 71.2 mm for the proposed planning method and 73.6 mm for clinician-defined planning, indicating that the proposed planning method provided a shorter and less invasive trajectory.

Figure 2 shows representative planning results for the same patient, comparing the proposed method with clinician-defined planning. The yellow region represents the tumor, and the surrounding boundary indicates the safety margin. The proposed planning result in Fig. 2(a) generated an ablation region that closely matched the safety margin, whereas the clinician-defined plan in Fig. 2(b) produced a substantially larger ablation region but achieved lower coverage of the margin-included target.

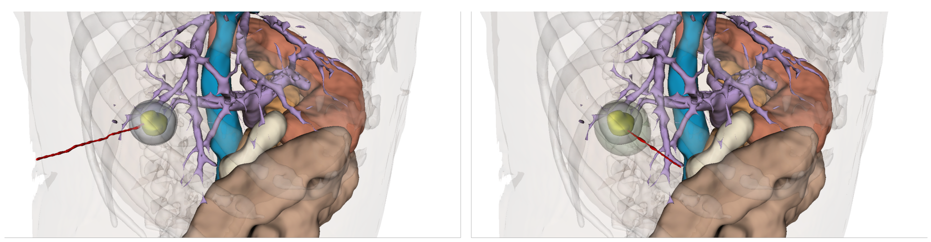

(a) (b)

Fig. 2. Representative treatment planning results comparing the antenna insertion trajectory and predicted ablation region between (a) the proposed method and (b) clinician-defined planning.

Clinical Feasibility Assessment The clinical applicability of the proposed planning method was evaluated by two MWA specialists using four categories: optimal, acceptable, indeterminate, and not feasible. Plans rated as optimal or acceptable were considered clinically applicable. As shown in Table 2, all antenna insertion trajectories were rated as optimal or acceptable by both clinicians, indicating clinically acceptable trajectory generation.

Table 1. Quantitative planning performance of the proposed and clinician-defined treatment plans across 13 patients. SD denotes standard deviation.

Patient	Tumor diameter (mm)	Proposed planning				Clinician planning			
		AE ↑	CP ↑	OD ↓	IPL ↓ (mm)	AE ↑	CP ↑	OD ↓	IPL ↓ (mm)
1	28	0.801	0.966	0.000	36.8	0.528	0.989	0.000	40.6
2	36	0.695	0.974	0.106	84.6	0.745	0.796	0.088	87.5
3	20	0.869	0.981	0.000	128.3	0.704	0.959	0.001	133.9
4	27	0.873	0.968	0.000	65.6	0.537	0.983	0.000	70.5
5	28	0.539	0.972	0.041	58.4	0.394	0.927	0.054	73.4
6	20	0.636	0.971	0.000	67.8	0.535	0.982	0.000	64.0
7	14	0.836	0.883	0.000	81.7	0.361	0.927	0.000	79.7
8	7	0.843	0.945	0.000	43.0	0.200	1.000	0.000	44.1
9	11	0.820	0.973	0.000	60.0	0.364	1.000	0.000	39.6
10	20	0.817	0.955	0.000	49.1	0.487	0.982	0.000	62.4
11	23	0.786	0.976	0.000	76.1	0.672	0.952	0.000	85.0
12	27	0.789	0.958	0.000	60.0	0.318	0.992	0.000	52.4
13	23	0.620	0.907	0.039	114.1	0.587	0.783	0.000	124.0
Mean	21.8	**0.764**	**0.956**	0.014	**71.2**	0.495	0.944	**0.011**	73.6
SD	7.9	0.106	0.029	0.031	26.4	0.162	0.073	0.027	29.3

Table 2. Clinician assessment of the feasibility of antenna insertion trajectory and time/power settings.

Evaluation item	Evaluator	Optimal	Acceptable	Indeterminate	Not feasible
Antenna insertion trajectory	Clinician 1	9	4	–	–
	Clinician 2	10	3	–	–
Time/power setting	Clinician 1	13	–	–	–
	Clinician 2	6	6	1	–

In contrast, greater inter-clinician variability was observed in the evaluation of treatment duration and power settings. This disagreement may reflect that multiple power–duration combinations can be clinically reasonable for the same target, depending on the balance among sufficient ablation coverage, treatment time, and the risk of excessive thermal damage. Therefore, the selection among these alternatives may be influenced by each clinician's experience, treatment preferences, and risk tolerance. One case was rated as indeterminate because of concern regarding potentially insufficient ablation, supporting the need for more explicit and quantitative criteria for treatment parameter selection.

3.3 Optimization Method Analysis

Table 3 compares the proposed GA with three gradient-free benchmark optimization methods to evaluate its optimization performance and computational efficiency. Random Search randomly generates and evaluates candidate solutions

Table 3. Quantitative comparison of optimization methods across 13 patients. Results are reported as the mean and SD.

Method	Statistic	AE ↑	CP ↑	OD ↓	IPL ↓ (mm)	Time ↓ (s)
Random Search	Mean	0.6654	0.9605	0.0245	70.08	49.21
	SD	0.1140	0.0331	0.0490	24.81	7.32
Bayesian TPE	Mean	0.7479	**0.9650**	0.0227	**65.30**	106.99
	SD	0.0920	0.0279	0.0559	24.13	6.98
CMA-ES	Mean	**0.7794**	0.9613	0.0228	67.35	54.82
	SD	0.0987	0.0269	0.0559	32.42	12.73
GA	Mean	0.7635	0.9560	**0.0143**	71.19	**42.74**
	SD	0.1061	0.0292	0.0313	26.36	5.53

within predefined search bounds. Tree-structured Parzen Estimator (TPE)-based Bayesian optimization selects subsequent candidate solutions using a probabilistic model constructed from previous evaluation results. Covariance Matrix Adaptation Evolution Strategy (CMA-ES) iteratively adjusts the sampling distribution of candidate solutions based on their evaluation results. For a fair comparison, the number of candidate evaluations was fixed at 2,400 for all methods, and model inference was performed only for candidates that passed the pre-inference hard-constraint screening.

Except for Random Search, all methods achieved similarly high AE values, and the mean AE values of all methods were higher than that of clinician-defined planning reported in Table 1. Although GA showed the lowest mean CP, the differences among the methods were small. GA also achieved the lowest OD, effectively limiting overlap with critical organs. In contrast, GA produced the longest IPL among the compared methods. Because each metric reflects a different planning objective, the superiority of an optimization method cannot be determined based on a single metric. Nevertheless, GA achieved the shortest overall optimization time while maintaining planning performance comparable to that of the other optimization methods, demonstrating its computational efficiency and practical advantages as the final planning method.

3.4 Comparison with Full Numerical Simulation

Planning Time Analysis Using the neural ablation prediction model as the forward model substantially reduced planning time. The model inference time was 16.3 ms per case, compared with an average of 10.8 s for full numerical simulation. The neural-network-based planning required an average of 42.7 s, including 1,664 forward evaluations taking 32.9 s. Performing the same number of evaluations with full numerical simulation would require approximately 17,971 s (5.0 h), indicating that the proposed framework enabled about 420-fold faster planning. All measurements were conducted on a GPU-enabled desktop with an AMD Ryzen 9 5900X CPU and an NVIDIA RTX 3090 GPU.

Table 4. Agreement between model-predicted and numerically simulated ablation zones for the optimizer-selected plans in 13 patients. CD denotes the centroid distance between the two ablation zones.

Evaluation aspect	Metric	Mean ± SD
Spatial overlap	Dice ↑	0.9108 ± 0.0375
	IoU ↑	0.8382 ± 0.0617
Spatial location	CD (mm) ↓	1.4674 ± 0.3435
Planning consistency	$\lvert\Delta\mathrm{AE}\rvert$ ↓	0.0404 ± 0.0309
	$\lvert\Delta\mathrm{CP}\rvert$ ↓	0.0432 ± 0.0553
	$\lvert\Delta\mathrm{OD}\rvert$ ↓	0.0061 ± 0.0123

Numerical Verification of Optimizer-Selected Plans Applying full numerical simulation directly within the optimization process is computationally impractical because of its high computational cost. However, neural network-based optimization may select solutions by exploiting prediction errors inherent in the model. Therefore, the final plan selected for each patient was re-evaluated using the full numerical simulation. As shown in Table 4, the model-predicted and numerically simulated ablation zones showed high spatial agreement, with a Dice score of 0.9108, an IoU of 0.8382, and a centroid distance of 1.4674 mm. The absolute differences in AE, CP, and OD were also small, at 0.0404, 0.0432, and 0.0061, respectively. These results indicate that the neural network predictions remained generally consistent with the full numerical simulation for the optimizer-selected plans.

4 Conclusion

In this study, we proposed a patient-specific MWA planning framework that combines a neural network-based ablation prediction model with a genetic algorithm. Trained on multiphysics simulation data, the model rapidly predicts ablation regions by incorporating tumor and vessel structures, antenna configuration, and treatment conditions. Compared with clinician-defined planning, the proposed method achieved higher ablation efficiency by reducing unnecessary ablation outside the target and shortened the antenna insertion trajectory, while maintaining broadly comparable target coverage and organ-damage levels. Most plans were also judged clinically applicable by MWA specialists.

However, because this study was conducted using a single dataset, external generalizability across different institutions and patient populations has not been sufficiently validated. In addition, the clinical applicability assessment was performed by only two MWA specialists and therefore may not fully reflect the treatment criteria and preferences of a broader group of clinicians. Although the optimizer-selected plans were independently verified using the full numerical simulation, prospective validation against actual post-ablation outcomes was not performed; therefore, their agreement with real clinical outcomes remains unconfirmed. Future studies should therefore include additional validation using independent multicenter clinical datasets, actual treatment outcomes, and a larger panel of clinicians.

Despite these limitations, the proposed framework enables planning approximately 420 times faster than full numerical simulation-based planning and demonstrates its potential as a fast digital twin-based system for quantitative, automated, and personalized MWA treatment planning.

Acknowledgments. This work was supported by the National Research Foundation of Korea (NRF) grant funded by the Korea government (MSIT) (No. RS-2024-00335185). This work was supported by the Korea Medical Device Development Fund grant funded by the Korea government (the Ministry of Science and ICT, the Ministry of Trade, Industry and Energy, the Ministry of Health & Welfare, the Ministry of Food and Drug Safety) (Project Number: RS-2026-25543484).

Disclosure of Interests. The authors have no competing interests to declare that are relevant to the content of this article.

References

1. An, C., Li, X., Zhang, M., Yang, J., Cheng, Z., Yu, X., Han, Z., Liu, F., Dong, L., Yu, J., et al.: 3d visualization ablation planning system assisted microwave ablation for hepatocellular carcinoma (diameter> 3): a precise clinical application. BMC cancer **20**(1), 44 (2020)
2. Antonelli, M., Reinke, A., Bakas, S., Farahani, K., Kopp-Schneider, A., Landman, B.A., Litjens, G., Menze, B., Ronneberger, O., Summers, R.M., et al.: The medical segmentation decathlon. Nature communications **13**(1), 4128 (2022)
3. Berjano, E.J.: Theoretical modeling for radiofrequency ablation: state-of-the-art and challenges for the future. Biomedical engineering online **5**(1), 24 (2006)
4. Cho, S., Seo, M., Shin, M., Yoon, K.: Towards digital twin of rf ablation: Real-time prediction of time-dependent thermal effects using transformer. In: International Workshop on Digital Twin for Healthcare. pp. 69–78. Springer (2025)
5. van Erp, G.C., Hendriks, P., Broersen, A., Verhagen, C.A., Gholamiankhah, F., Dijkstra, J., Burgmans, M.C.: Computational modeling of thermal ablation zones in the liver: a systematic review. Cancers **15**(23), 5684 (2023)
6. Frackowiak, B., Van den Bosch, V., Tokoutsi, Z., Baragona, M., de Greef, M., Elevelt, A., Isfort, P.: First validation of a model-based hepatic percutaneous microwave ablation planning on a clinical dataset. Scientific Reports **13**(1), 16862 (2023)
7. Gao, H., Wang, X., Wu, S., Zhou, Z., Bai, Y., Wu, W.: Conformal coverage of liver tumors by the thermal coagulation zone in 2450-mhz microwave ablation. International Journal of Hyperthermia **36**(1), 590–604 (2019)
8. Gorman, J., Tan, W., Abraham, J.: Numerical simulation of microwave ablation in the human liver. Processes **10**(2), 361 (2022)
9. Gu, H., Seo, Y., Chung, D.J., Paik, K.Y., Yoon, S.K., Lim, J.: Microwave ablation vs. liver resection for patients with hepatocellular carcinomas. Journal of liver cancer **25**(1), 99–108 (2025)

10. Heshmat, A., O'Connor, C.S., Albuquerque Marques Silva, J., Paolucci, I., Jones, A.K., Odisio, B.C., Brock, K.K.: Using patient-specific 3d modeling and simulations to optimize microwave ablation therapy for liver cancer. Cancers **16**(11), 2095 (2024)
11. Keshavamurthy, K.N., Eickhoff, C., Ziv, E.: Pre-operative lung ablation prediction using deep learning. European Radiology **34**(11), 7161–7172 (2024)
12. Kim, Y.s., Lee, W.J., Rhim, H., Lim, H.K., Choi, D., Lee, J.Y.: The minimal ablative margin of radiofrequency ablation of hepatocellular carcinoma (>2 and<5 cm) needed to prevent local tumor progression: 3d quantitative assessment using ct image fusion. American Journal of Roentgenology **195**(3), 758–765 (2010)
13. Li, S., Zhou, F., Zhang, Y., Xu, S., Wang, Y., Cheng, L., Bie, Z., Li, B., Li, X.G.: Multi-stage automatic and rapid ablation and needle trajectory planning method for ct-guided percutaneous liver tumor ablation. Medical Physics **52**(1), 113–130 (2025)
14. Liu, F., Liang, P., Yu, X., Lu, T., Cheng, Z., Lei, C., Han, Z.: A three-dimensional visualisation preoperative treatment planning system in microwave ablation for liver cancer: a preliminary clinical application. International Journal of Hyperthermia **29**(7), 671–677 (2013)
15. Marrero, J.A., Kulik, L.M., Sirlin, C.B., Zhu, A.X., Finn, R.S., Abecassis, M.M., Roberts, L.R., Heimbach, J.K.: Diagnosis, staging, and management of hepatocellular carcinoma: 2018 practice guidance by the american association for the study of liver diseases. Hepatology **68**(2), 723–750 (2018)
16. Meister, F., Audigier, C., Passerini, T., Lluch, È., Mihalef, V., Maier, A., Mansi, T.: Fast automatic liver tumor radiofrequency ablation planning via learned physics model. In: International Conference on Medical Image Computing and Computer-Assisted Intervention. pp. 167–176. Springer (2022)
17. Nahmed, I., Dettori, F., Verde, J., Duprez, M., Alvarez, P., Cotin, S.: A digital twin for microwave liver treatment replanning. International Journal of Computer Assisted Radiology and Surgery pp. 1–8 (2026)
18. Perez, E., Strub, F., De Vries, H., Dumoulin, V., Courville, A.: Film: Visual reasoning with a general conditioning layer. In: Proceedings of the AAAI conference on artificial intelligence. vol. 32 (2018)
19. Radjenović, B., Sabo, M., Šoltes, L., Prnova, M., Čičak, P., Radmilović-Radjenović, M.: On efficacy of microwave ablation in the thermal treatment of an early-stage hepatocellular carcinoma. Cancers **13**(22), 5784 (2021)
20. Seo, M., Shin, M., Noh, G., Yoo, S.S., Yoon, K.: Multi-modal networks for real-time monitoring of intracranial acoustic field during transcranial focused ultrasound therapy. Computer Methods and Programs in Biomedicine **257**, 108458 (2024)
21. Shin, M., Seo, M., Cho, S., Park, J., Kwon, J.H., Lee, D., Yoon, K.: Physrfanet: Physics-guided neural network for real-time prediction of thermal effect during radiofrequency ablation treatment. Engineering Applications of Artificial Intelligence **138**, 109349 (2024)
22. Simon, C.J., Dupuy, D.E., Mayo-Smith, W.W.: Microwave ablation: principles and applications. Radiographics **25**(suppl_1), S69–S83 (2005)
23. Tan, J., Tang, T., Zhao, W., Zhang, Z.S., Xiao, Y.D.: Initial incomplete thermal ablation is associated with a high risk of tumor progression in patients with hepatocellular carcinoma. Frontiers in oncology **11**, 760173 (2021)
24. Wasserthal, J., Breit, H.C., Meyer, M.T., Pradella, M., Hinck, D., Sauter, A.W., Heye, T., Boll, D.T., Cyriac, J., Yang, S., et al.: Totalsegmentator: robust segmentation of 104 anatomic structures in ct images. Radiology: Artificial Intelligence **5**(5), e230024 (2023)

25. Yang, S., Ni, H., Zhang, A., Zhang, J., Zang, H., Ming, Z.: Impact of postoperative morbidity on the prognosis of patients with hepatocellular carcinoma after laparoscopic liver resection: a multicenter observational study. Scientific Reports **15**(1), 1724 (2025)
26. Zhang, R., Wu, S., Wu, W., Gao, H., Zhou, Z.: Computer-assisted needle trajectory planning and mathematical modeling for liver tumor thermal ablation: A review. Mathematical biosciences and engineering **16**(5), 4846–4872 (2019)